ACS Biomaterials SCIENCE & ENGINEERING

pubs.acs.org/journal/abseba

Article

Rheological Characterization and 3D Fabrication of Artificial Bacterial Biofilms

Annie Scutte, Kiram Harrison, Tyler Gregory, David Quashie, Jr., Subramanian Ramakrishnan, and Jamel Ali*

Cite This: *ACS Biomater. Sci. Eng.* 2025, 11, 3455−3466

Read Online

ACCESS | Metrics & More | Article Recommendations | Supporting Information

ABSTRACT: Biofilms are significantly involved in the progression of many diseases, such as cancer and upper respiratory infections, due to their ability to adhere to soft tissues. Factors influencing biofilm development have been extensively studied on planar substrates; however, there is limited understanding regarding biofilm growth and interactions within 3D matrices. Developing biofilm models that closely mimic natural bacterial communities' chemical and mechanical properties in soft tissues is essential for developing next-generation antibacterial compounds and therapeutics, as 3D biofilms are more complex and less susceptible to treatment than their 2D counterparts. Here, to understand environmental viscoelastic effects on biofilms within 3D matrix environments, two types of alginate-based hydrogels are formulated and used to encapsulatevarying concentrations of *Salmonella* Typhimurium. We explore the effects of increasing *S.* Typhimurium concentrations on hydrogel rheological properties and assess the impact of printing parameters on bacterial viability. Results show that hydrogels exhibit shear thinning behavior and that increasing the bacterial concentration up to 1×10^7 CFU mL^{-1} has no significant effect on the hydrogel precursor moduli and low shear viscosity. However, increasing the bacterial concentration to 1×10^{10} CFU mL^{-1} significantly decreases the hydrogel shear viscosity and modulus. Utilizing extrusion-based bioprinting, the optimal printing parameters (Pr > 0.8) have minimal effects on bacterial viability (>80%) over a 4 day incubation period. Additionally, we find that lower concentrations of bacteria form larger aggregates over time than hydrogels with higher cell concentrations. We show that biofilm growth in 3D depends on both initial bacterial density and matrix rigidity. Further development of physicochemically tuned bioprinted bacterial communities will aid our understanding of bacterial interactions within their 3D environments and enable the use of *in vitro* tissue models that incorporate biofilms for high-throughput therapeutic screening.

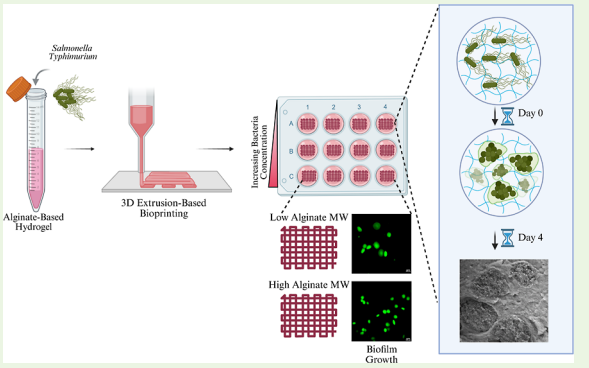

KEYWORDS: *3D printing, biofilms, rheology, bacterial aggregates*

1. INTRODUCTION

Over the past several decades, it has become widely accepted that many bacteria do not primarily exist in a planktonic state but spend most of their existence as cellular aggregates known as biofilms.[1,2] Biofilms exist as intricate communities of bacteria surrounded by self-produced extracellular polymeric substances (EPS) that are composed of excreted proteins, extracellular DNA, and cellular debris,[2] which allows these microorganisms to survive harsh environmental conditions and enhance their nutrient accessibility.[2] The formation of bacterial aggregates is influenced by factors such as nutrient availability, pH, temperature, quorum sensing, stress, and substrate characteristics.[3,4] As a natural mode of subsistence for many prokaryotes, biofilms can also consist of single or mixed bacterial species, allowing them to exhibit heightened resistance to antimicrobial therapies and immune defenses, thus posing an imminent threat to human health.[5] This resilience is often associated with infections and chronic diseases like cystic fibrosis or cancer.[6−8] Biofilms colonize biotic and abiotic surfaces such as indwelling implants (i.e., catheters, prosthetics, or heart valves) and soft tissues (i.e., lungs, skin, oral cavities).[6] For instance, *Salmonella* Typhimurium is a Gram-negative bacterium often contracted through contaminated food or water. This human pathogen is primarily known to colonize the gallbladder epithelium and can result in serious complications such as intestinal bleeding and can become fatal if left untreated.[3,8] Cells within *S.* Typhimurium biofilms can also disseminate to various soft tissues and organs like lymphoid tissue, liver, and spleen.[3,8−10] Previous

Received: February 3, 2025
Revised: May 5, 2025
Accepted: May 6, 2025
Published: May 16, 2025

https://doi.org/10.1021/acsbiomaterials.5c00223
ACS Biomater. Sci. Eng. 2025, 11, 3455−3466

investigations have highlighted some of the biochemical and biophysical factors influencing natural biofilm growth;[11−14] however, there remains a pressing need to understand the mechanisms underlying biofilm formation in artificial systems that replicate both the chemical and mechanical properties of natural bacterial communities found in soft tissues, which is crucial for developing new therapeutic strategies.

Biofilms of various bacterial strains have been extensively grown on planar substrates such as agar, glass, and polymer surfaces.[15−18] These investigations have expanded our understanding of the factors influencing biofilm growth, such as nutrient diffusion, substrate stiffness, cell−cell interactions, and mechanical deformation. For instance, Fei et al. researched *Vibrio cholerae* biofilms and demonstrated that the morphodynamics of these biofilms strongly depend on the stiffness of the agar substrate they are grown.[15] Results from this investigation demonstrated that biofilms exhibited elastic behavior similar to hydrogels but also displayed strong adhesion on the agar substrates. As the initially smooth biofilm expanded on different agar substrates, mechanical stresses developed within the biofilm due to friction with the agar surface, resulting in a transition to wrinkled patterns caused by mechanical instability.[15] Current work has shifted to understanding biofilm growth in hydrogel systems. Recently, Asp et al. investigated the correlation between substrate stiffness and the development of *Serratia marcescens* biofilms by cultivating them on synthetic hydrogel substrates with tunable mechanical properties.[11] In contrast to growth on agar, Asp et al. found that *S. marcescens* biofilms exhibited increased growth with higher substrate stiffness. Similarly, Wang et al. demonstrated that the growth of the pathogenic biofilm *Pseudomonas aeruginosa* on stiffer agarose gels resulted in higher surface adhesion and accumulation compared to softer gels.[18] Although valuable insights are acquired from agar-based studies regarding biofilm growth patterning, investigating biofilms on agar or polymer-derived solid−air interfaces has limitations, as they fail to mimic the complexities of biofilm growth in 3D matrices.[11,19,20]

Biofilms associated with chronic infections are often found as non-surface-attached bacterial aggregates embedded in hydrated polymer-rich environments.[21−24] Previous work has demonstrated morphodynamical differences between biofilm formation in 2D compared to confined 3D environments, which play an essential role in bacterial susceptibility to antimicrobial compounds.[20] Initial work aiming to understand bacteria biofilm development in 3D environments has been shown to have more physiological relevance when compared to chronic infection-associated biofilms.[25] Early work by Coquet et al. demonstrated that *P. aeruginosa* exhibited more physiologically relevant biofilm properties when encapsulated in alginate hydrogel matrices with increased drug resistance.[25] However, some limitations of these investegations included gradient nutrient and oxygen access in the hydrogel systems, resulting in larger biofilms forming toward nutrient and oxygen interfaces.[23,25] To address some of these limitations, 3D bioprinting serves as a promising technique that allows for the biofabrication of complex porous structures, with high spatial resolution and control.[26] These techniques have been widely used to fabricate cell-laden bioinks rapidly and for various applications such as tissue engineering and drug screening.[26−28] Extrusion-based bioprinting is one of the most common 3D printing methods due to a lack of biomaterials compatible with other printing methods. Gelatin and alginate are widely used natural polymers for tissue engineering applications due to their compositional similarities to the native ECM.[29] Unlike extrusion-based applications for tissue engineering applications, 3D bioprinting biofilms or living material (LM) platforms using naturally derived polymers are still emerging.[30] Previous work has explored the feasibility of fabricating 3D biofilms or LM models for applications ranging from drug screening to bioremediation.[31,32] In works by Aliyazdi et al., alginate-based *Escherichia coli* biofilms were biofabricated to serve as an *in vitro* infection model.[33] 3D bioprinting of bacteria is vital to understanding the nature of biofilm formation in 3D constructs for novel therapeutic development.[26,34]

One of the challenges presented in the development of bioinks for 3D bioprinting is understanding the effects of high cell densities on the hydrogel rheological properties, which affects printing feasibility.[35] It has been shown that the incorporation of cells affects the rheological properties of the hydrogels and hydrogel printability for mammalian cells in different hydrogel systems.[35,36] While there have been reports exploring the effects of viscoelastic properties of biofilms grown on 2D substrates, much remains unknown about the mechanics of bacteria confined in 3D structured environments, in contrast to what has been established for mammalian cells cultured in 3D matrices.[37] Kandemir et al. demonstrated the effects of the bacterial growth medium on the rheological properties of agarose hydrogels when encapsulated with two different bacterial strains.[38] This investigation highlights the role of nutrient accessibility in the viscoelasticity of bacterium-based hydrogels. While it is now known that there is a drastic contrast in the morphology of biofilms grown in 2D compared with 3D structured environments, much is still unknown about the effects of environmental viscoelastic properties on physical biofilm growth in 3D structured environments. Rheological measurements have shown that biofilms developed under different ecological conditions have a high variability in their viscoelastic nature over a range of length scales. Recent work by Jana et al. demonstrated that biofilms of various species exhibit different viscoelastic properties under large-amplitude oscillatory shear (LAOS) conditions due to the excretion of different macromolecules and biopolymers during biofilm formation.[39] Understanding the mechanics of biofilms in response to their environment is pertinent to correlating biofilm-based infections to their resistance to antibiotics.

Here, we investigate the use of extrusion-based bioprinting to generate 3D bacterial biofilm models under tissue-like culture conditions. We examine how increasing bacterial concentration affects the hydrogel rheological properties and printability. Using two alginate-based hydrogels, we encapsulated the Gram-negative bacterium *S.* Typhimurium at varying concentrations. The alginates used in this investigation vary in molecular weight; however, hydrogels are formulated to exhibit similar rheological properties before crosslinking. Then, we also explore the effects of polymer molecular weight and initial bacterial cell density on viability, aggregate formation, and morphology. We show that the varying concentrations of *S.* Typhimurium have no significant effect on the rheological properties of the two alginate-based hydrogel precursors. Both hydrogels were formulated to be highly printable. The 3D-printed biofilms reported may serve as a platform for investigating pathogenic bacterial interactions in soft tissue-like materials for future high-throughput drug screening applications.

https://doi.org/10.1021/acsbiomaterials.5c00223
ACS Biomater. Sci. Eng. 2025, 11, 3455−3466

2. MATERIALS AND METHODS

2.1. Hydrogels' Formulation. The following materials used for hydrogel formulation were obtained from Sigma-Aldrich: alginate (alginic acid sodium salt, low viscosity: 4−12 cP, 1% in H_2O at 25 °C; medium viscosity: >2000 cP, 2% in H_2O at 25 °C); gelatin (gel strength ∼300 g Bloom, type A form porcine skin); calcium chloride ($CaCl_2$, anhydrous, granular, ≤7.0 mm, ≥93.0%); and Dulbecco's modified Eagle's medium—low glucose (DMEM-low glucose medium). The molecular weight of the two types of alginates used was previously determined to be 24 kDa (LA) and 773 kDa (MA) for low- and medium-viscosity alginate, respectively.[40] Alginate−gelatin hydrogels were prepared by first dissolving gelatin in DMEM for 1 h at a mixing speed of 400 rpm at 50 °C. Then, alginate was dissolved in the gelatin solution for 3 h at 400 rpm at 50 °C. Alginate−gelatin hydrogel solutions were then transferred to 50 mL centrifuge tubes and centrifuged at 1000*g* for 10 min to remove entrapped bubbles in the mixture. Hydrogels were stored at 4 °C until they were ready to be used. For hydrogel characterization assessments, a final concentration of 5% (w/v) alginate (LA) and 5% (w/v) gelatin hydrogel blends were formulated. For high-molecular-weight alginate-based hydrogels, the final hydrogel composition was 1.5% (w/v) alginate (MA) and 5% (w/v) gelatin. Three batches of each hydrogel blend were prepared to account for batch-to-batch variability (n = 3).

2.2. Inoculation of Hydrogels. *S.* Typhimurium was taken from a glycerol (50% (v/v)) stock solution and inoculated in 20 mL of LB broth (1% (w/v) tryptone, 0.5% (w/v)yeast, 1% (w/v) NaCl). The bacteria were aerated in an incubator shaker at 37 °C and 120 rpm. The cultures were harvested in the early log phase after 3−5 h of cultivation. The concentration of bacteria was measured using optical density at a wavelength of 600 nm to achieve a concentration of 1×10^8 CFU mL^{-1} (OD_{600} = 1.00). The bacteria were transferred to 1.7 mL centrifuge tubes and collected by centrifugation at 10,000*g* and 4 °C for 10 min. Then, the bacterial pellet was washed twice in sterilized PBS to remove residual LB medium. The bacterial pellet was re-suspended in 1 mL of sterilized deionized water and was diluted three times to achieve bacterial concentrations of 1×10^5, 1×10^6, and 1×10^7 CFU mL^{-1}. The series of diluted bacterial concentrations were collected by centrifugation (10,000*g*, 4 °C for 10 min) and re-suspended in 50 μL of sterilized deionized water and added to 3 mL of alginate-gelatin hydrogels, which were previously warmed at 37 °C. To achieve a higher concentration of bacteria, a larger volume was cultured under the same conditions previously stated and concentrated to reach a final concentration of 1×10^{10} CFU mL^{-1}. The bacterial suspension was well mixed in the hydrogel by repeated gentle mixing with a micropipet, producing 3 mL of bacterial bioink.

2.3. Hydrogel Rheological Characterization. The rheological properties of acellular hydrogel formulations were obtained using an MCR 302 Anton Paar Rheometer. A 25 mm-diameter parallel-plate geometry (PP25/S) with a 1 mm gap distance was used for all measurements. Before all rheological experiments were conducted, hydrogels were warmed to 37 °C for 1 h, and then the samples were loaded onto the rheometer and were pre-sheared at a constant shear rate of 50 s^{-1} at 37 °C for 60 s to remove hysteresis within the polymer network. The first test conducted was an isothermal time sweep to determine the gelation time for each hydrogel. An isothermal time sweep was conducted at a constant oscillation frequency of 1 Hz and a constant amplitude strain of 0.1% for 60 min at 25 °C. Following the isothermal time sweep, a new sample was loaded onto the rheometer to limit long-term evaporation losses, pre-sheared, and then equilibrated to 25 °C for 30 min. Following hydrogel equilibration, storage and loss moduli were measured as a function of frequency. Oscillatory measurements were performed at a constant amplitude of 0.1% and a frequency range of 0.05−25 Hz. Then, viscosity as a function of the shear rate was measured in the shear rate range of 1−50 s^{-1}. Shear rheology data were then fit to the power law model (eq 1)

$$\eta = k \times \dot{\gamma}^{-n} \tag{1}$$

where η, k, $\dot{\gamma}$, and n represent the viscosity, flow consistency index, shear rate, and flow behavior index, respectively. Hydrogel rheological measurements were conducted three times for three different hydrogel batches to account for batch variability. The same rheological measurements were then performed for bacterium-laden hydrogels to assess the effects of bacterial loading on hydrogel properties. To determine the modulus of the crosslinked hydrogels, samples were loaded onto the rheometer at 37 °C, pre-sheared, and allowed to equilibrate at 25 °C for 30 min. The modulus of un-crosslinked hydrogels was measured for 3 min before ionic crosslinking with a 5% (w/v) $CaCl_2$ solution. Hydrogels were crosslinked for 4 min and then rinsed twice with PBS. The modulus of crosslinked hydrogels was measured for 3 min at 25 °C. Then, the temperature was increased to 37 °C, and the hydrogel modulus was measured for 20 min under isothermal conditions. Lastly, stress relaxation measurements were conducted on crosslinked hydrogel samples at a constant strain of 10% for a duration of 1000 s. The stress relaxation times for the hydrogels were obtained using the generalized Maxwell equation with i elements in parallel (eq 2)

$$G(t) = G_\infty + \sum_{i=1} G_i \exp\left(-\frac{t}{\tau_i}\right) \tag{2}$$

G_∞ is the equilibrium shear relaxation modulus, G is the shear relaxation modulus, t is time, and τ_i is the relaxation time of the ith relaxation process.

2.4. Bioprinting. 3D extrusion-based bioprinting was done using SunP Biomaker V2. Hydrogels were printed as 10 × 10 × 1 mm constructs predesigned using CAD software with rectilinear infill patterns, an infill density of 20%, and a layer height of 0.5 mm. Acellular hydrogels were loaded in a 3 mL syringe and printed using a 22-gauge tapered-tip needle (ID = 0.41 mm) at 25 °C. To characterize the hydrogel printability, hydrogel samples were printed in layers onto a 1 mm-thick glass slide and imaged to assess strand width and pore sizes. Three initial seeding concentrations of *S.* Typhimurium (1×10^5, 10^6, 10^7 CFU mL^{-1}) were investigated for printing bacterium-laden constructs. Desired bacterial concentrations were pelleted, re-suspended in 50 μL of 1× PBS, added to 3 mL of the hydrogel solution, and mixed with a stereological pipet by aspirating up and down. Bacterium-laden hydrogel scaffolds were printed at a print speed of 5 mm s^{-1} and an extrusion rate of 0.6 mm^3 s^{-1}. Bioprinted constructs were crosslinked using a 5% (w/v) $CaCl_2$ solution for 4 min, rinsed twice with the PBS solution, and incubated in DMEM supplemented with 10% FBS at 37 °C and 5% CO_2. Bacterium-laden constructs were then imaged over a 4 day culture period.

2.5. Fluorescence Staining for Biofilm Viability. Viability was assessed using a Baclight Live/Dead Viability/Cytotoxicity assay consisting of a 3:1 ratio of SYTO9 and propidium iodide. Staining was carried out every day for a 4 day incubation period following bioprinting. Samples were washed twice with PBS following culture medium removal and then incubated with the staining solution at 37 °C for 15−20 min. Imaging acquisition was conducted immediately after incubation using a Nikon Eclipse Ti2 inverted microscope using 10× and 20× objectives. Images obtained using the 10× objective were used for viability assessment, as it provided a wider field of view, and images obtained using the 20× objective were analyzed for average aggregate size development over time. All images were denoised to remove any noise or debris in images using Nikon Instruments analysis software. Bacterial viability was quantified using ImageJ1.52a, which generates a z-projection image from the z-stacks of stained bacteria within the bioprinted models. The viability of bacteria was measured by dividing the area of green fluorescence by the total area. Staining was repeated for three different hydrogel batches, and 4 images from different locations of the printed construct were analyzed for each sample (n = 3).

2.6. Scanning Electron Microscopy. To prepare bacterium-laden constructs for SEM imaging, samples were washed with PBS to remove waste and detached bacterial cells. Then, samples were fixed in a 2.5% (v/v) glutaraldehyde solution for 30 min. Samples were

https://doi.org/10.1021/acsbiomaterials.5c00223
ACS Biomater. Sci. Eng. 2025, 11, 3455−3466

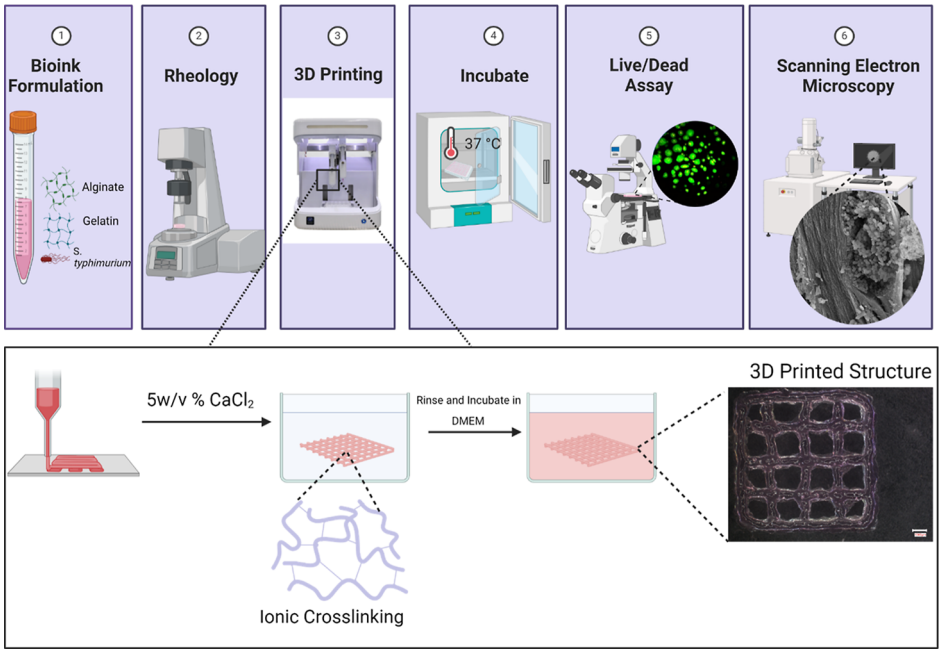

Figure 1. Schematic of *S.* Typhimurium hydrogel fabrication and characterization. Hydrogel precursors were formulated using two different MW alginates and encapsulated with varying concentrations of *S.* Typhimurium. Hydrogels were characterized using rheology to assess the viscoelastic properties with and without the addition of *S.* Typhimurium. Gels are 3D printed and crosslinked with 5 w/v %$CaCl_2$ and assessed for bacterial viability and structural organization using fluorescent live/dead cytotoxicity assays and electron microscopy. [Figure generated in BioRender.]

then dehydrated using ethanol series dehydration of the following concentrations (10, 25, 30, 50, 70, 80, 90, 95, and 100% (v/v)) for 10 min for each concentration. Then, samples were further dehydrated in 50% (v/v) HDMS in 100% ethanol and 100% HDMS for 5 min after ethanol dehydration and allowed to air dry overnight.[41−43] Samples were cross-sectioned using a fine-tip blade and coated with gold at a 20−30 nm thickness. Samples were imaged using the Phenom XL Q2 Desktop SEM at 10 kV and 10 Pa.

2.7. Statistical Analysis. All experiments were conducted in triplicate ($n = 3$), and all statistical analysis was done using GraphPad Prism version 8.0. Significance was checked for the bacteria microcolony area via two-way ANOVA with Tukey's multiple comparison test. Statistical significance was defined as $*p < 0.05$ $**p < 0.01$, $***p < 0.001$, $****p < 0.0001$.

3. RESULTS

3.1. Rheology of Hydrogels. Hydrogels were formulated using alginate and gelatin (Figure 1), where the alginates used varied in MW. The molecular weight of the alginates used was previously reported to be 24 kDa (5%LA−5%Gel) and 773 kDa (1.5%LA−5%Gel).[40] Hydrogels were formulated to exhibit similar rheological properties before crosslinking with $CaCl_2$. In Figure 2a, we show the gelation kinetics of the two types of hydrogels used, where the storage and loss moduli are recorded over time at 25 °C. Hydrogel precursors were formulated to have similar properties, where the storage and loss modulus of the two gel types are within the same order of magnitude. Due to the differences in solid content and alginate MW, hydrogels exhibit different gelation times (circled in red in Figure 2a), where the crossover point between the storage and loss modulus for the 5−%Gel and 1.5%MA−5% Gel hydrogel precursors was observed at 6 and 12 min, respectively. Next, frequency sweeps were conducted to determine the viscoelastic behaviors of both gel types. Both gel types have viscoelastic solid-like behavior, where the storage modulus is greater than the loss modulus ($G' > G''$) as frequency increases, as shown in Figure 2b. This figure also shows that both gel types exhibit similar storage and loss moduli at higher frequency ranges (1−25 Hz). Shear rheology measurements in Figure 2c depict that both gels exhibit shear-thinning behaviors with flow behavior index (n) values of 0.87 and 0.81 for 5%LA−5%Gel and 1.5%MA−5%Gel gels, respectively, which indicates that the viscosity of both gel types decreases as the shear rate increases.

Next, we assessed the rheological properties of both gels once crosslinked with a 5% $CaCl_2$ solution, which allows for the physical crosslinking between the divalent cations and the carboxyl groups of the alginate,[44] and maintained them at 37 °C as depicted in Figure 2d. The 5%LA−5%Gel hydrogel exhibited a crosslinked storage modulus approximately twice that of the 1.5%MA−5%Gel hydrogel, where the crosslinked modulus was 4.74 and 2.73 kPa, respectively (Figure S1). This indicates that the 5%LA−5%Gel hydrogel can form more interconnected networks due to the difference in polymer chain length and polymer content compared to the 1.5%MA−5%Gel hydrogels. Lastly, we show the stress relaxation behavior of both hydrogels in Figure 2e at a constant strain of 10%. The stress relaxation modulus is normalized to the elastic relaxation modulus (G_0) at the strain's initial time of $t = 0$, increasing by 10%. By fitting the experimental stress relaxation data to the generalized Maxwell equation (eq 2), the best-fit parameters obtained indicated that both hydrogels have three distinct stress relaxation processes, and all fitting parameters are provided in Table S1. From the model fit, Figure 1e shows that at a constant applied strain of 10%, the 1.5%MA−5%Gel retains a larger fraction of its initial stress (∼39%) compared to the 5%LA−5%Gel, which only retains 25%. Thus, this shows that 1.5%MA−5%Gel is more resilient and maintains its structural integrity over time. Next, we also see from the fitting parameter that, initially, the 5%LA−5%Gel retains more stress given by the first relaxation modulus; however, the longtime relaxation time (τ_1) is higher for the

https://doi.org/10.1021/acsbiomaterials.5c00223
ACS Biomater. Sci. Eng. 2025, 11, 3455−3466

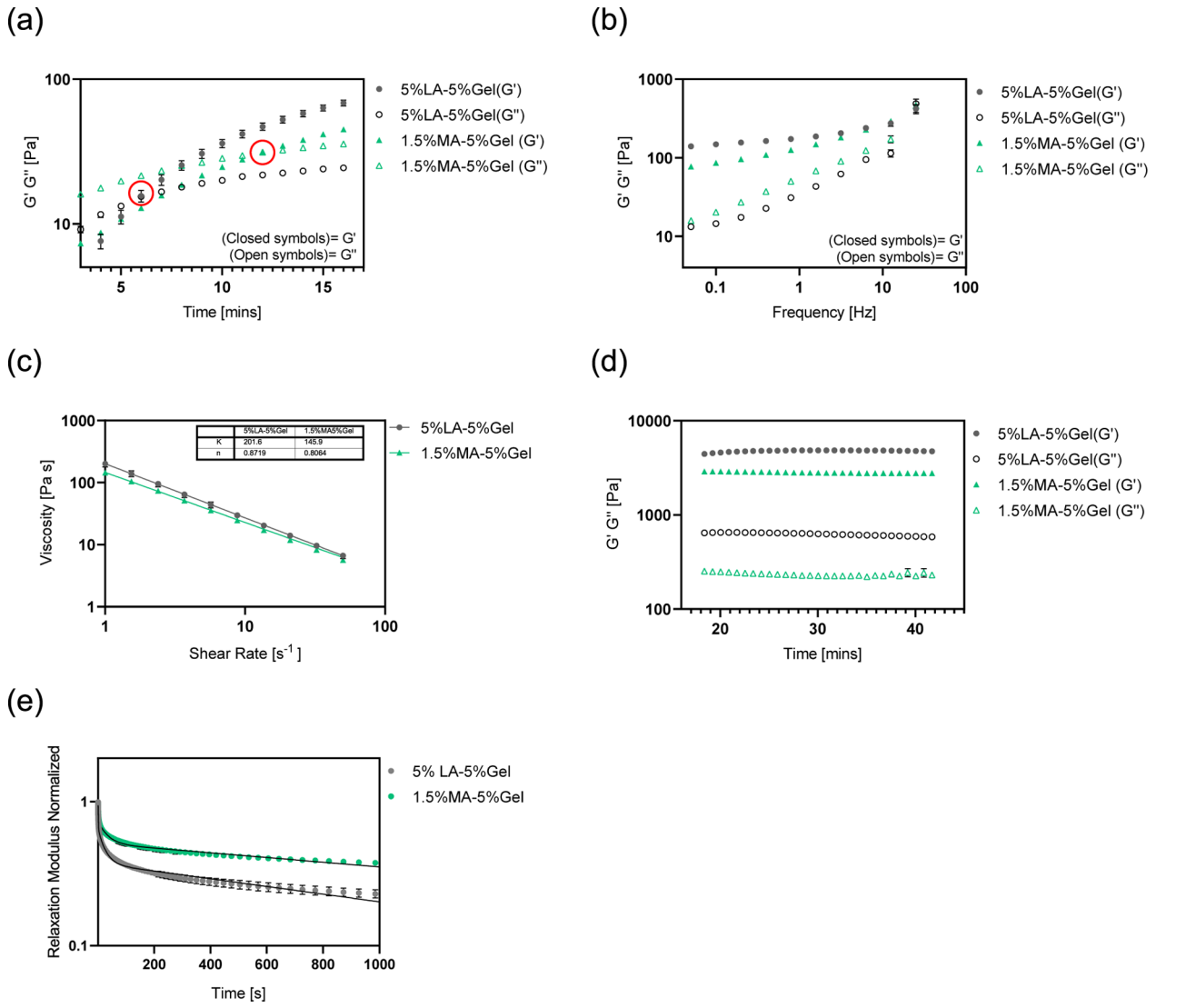

Figure 2. Rheologicalcharacteristics of hydrogel precursors without bacterial encapsulation. (a) A comparison of hydrogels' gelation kinetics of hydrogels depicts that 5%LA−5%Gel hydrogels have a faster gelation rate (6 min) than the 1.5%MA−5%Gel hydrogels (12 min). Gelation points are circles in red. (b) Frequency sweep shows that both hydrogel precursors exhibit viscoelastic solid-like behaviors and have similar properties. (c) Both gels exhibit shear thinning behaviors with similar shear viscosities. (d) After crosslinking with $CaCl_2$, the 5%LA−5%Gel storage modulus is approximately twice that of the 1.5MA−5%Gel hydrogel. (e) Stress relaxation measurements fitted to the generalized Maxwell equation show that 5%LA−5%Gel has a faster stress relaxation time than the 1.5MA−5%Gel hydrogel.

1.5%MA−5%Gel (∼11.52 s) suggesting that it relaxes more slowly than the 5%LA−5%Gel (∼9.2 s). We also see a slower intermediate relaxation process (τ_2) for the 1.5%MA−5%Gel than the 5%LA−5%Gel. Overall, the 5%LA−5%Gel has a faster stress relaxation behavior than the 1.5%MA−5%Gel, which may be attributed to the alginate polymer molecular weights in both hydrogels, which is consistent with observations in previous literature showing that lower polymer molecular weight contributes to faster relaxation behavior compared to higher polymer molecular weight.[45]

3.2. Rheology of Hydrogels with Varying Concentrations of Encapsulated Bacteria. Hydrogels were encapsulated with four different concentrations of *S.* Typhimurium (1×10^5, 1×10^6, 1×10^7, and 1×10^{10} CFU mL^{-1}) and assessed to determine the effects of bacterial loading on the viscoelastic properties of hydrogel precursors at 25 °C. Results shown in Figure 3 depict that as the bacterial concentration increases up to 1×10^7 CFU mL^{-1}, the modulus of both hydrogels is not significantly affected compared to the modulus of hydrogels without bacterial encapsulation. However, we note that at a concentration above 1×10^{10} CFU mL^{-1}, hydrogels' storage (G') and loss modulus (G'') decrease when compared to those with lower bacterial concentrations. We also show the frequency sweep of collected bacterial paste, obtained by centrifugation of saturated bacterial cultures, consisting mainly of log-phase bacteria with polysaccharides, proteins, DNA, and cellular debris. Results show that the modulus of bacterial paste is orders of magnitude stiffer than that of the hydrogels and behaves more like an elastic solid. This indicates that at much higher concentrations of bacteria, the hydrogels' microstructure is significantly altered compared to lower bacterial concentrations. We also show that at lower bacterial densities, the shear thinning behavior of the hydrogels remains unchanged, where the deformation rate of the hydrogel is similar to that of hydrogels without bacterial encapsulation. However, at a higher bacterial concentration,

https://doi.org/10.1021/acsbiomaterials.5c00223
ACS Biomater. Sci. Eng. 2025, 11, 3455−3466

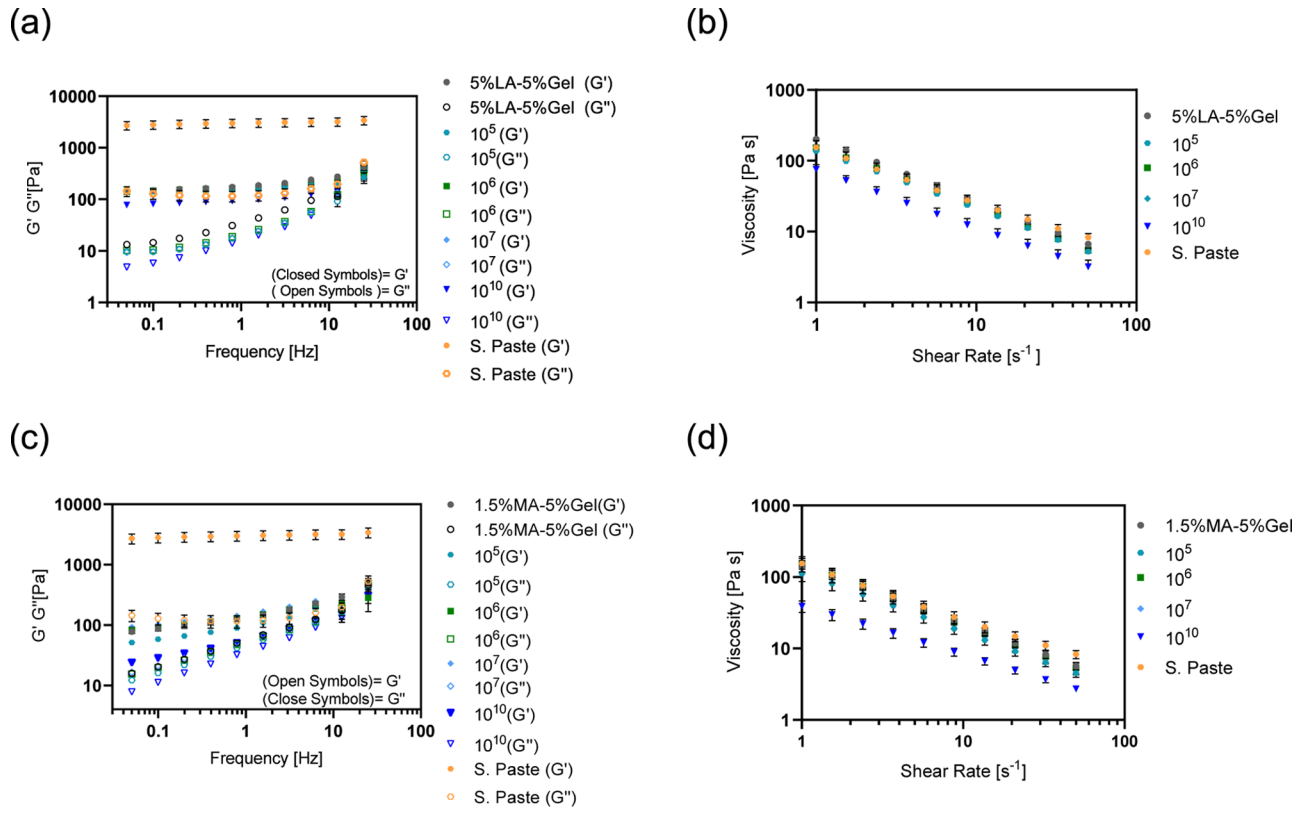

Figure 3. Rheology of hydrogel precursors encapsulated with varying concentrations of *S.* Typhimurium. (a) Frequency sweep of 5%LA5%Gel encapsulated with *S.* Typhimurium concentrations of 1×10^5, 1×10^6, 1×10^7, and 1×10^{10} CFU mL^{-1}. (b) Flow curve of increasing bacterial concentration on 5%LA−5%Gel. (c) Frequency sweep of 1.5%MA−5%Gel encapsulated with *S.* Typhimurium concentrations of 1×10^5, 1×10^6, 1×10^7, and 1×10^{10} CFU mL^{-1}. (d) Flow curve of increasing bacterial concentration on 5%LA−5%Gel.

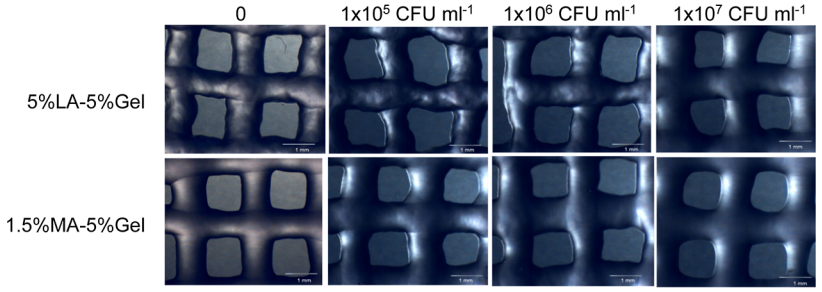

Figure 4. Effects of increasing bacterial concentrations on the printability of both 5%LA−5%Gel and 1.5%MA−5%Gel hydrogels. All structures were printed at a print speed of 5 mm s^{-1} and 0.6 mm^3 s^{-1} at 25 °C. Images show that increasing bacterial concentration had a minimal impact on the printed hydrogel pore structure (scale bar = 1 mm).

the hydrogel becomes more shear-thinning compared to hydrogels encapsulated with lower bacterial concentrations. Lastly, we performed the same rheological mesurments on a concentrated volume of cells obtained from the mid-exponential phase at OD_{600} = 1 (*S.* Paste). We observed that the collected bacterial paste exhibited a shear thinning behavior similar to that of the neat hydrogels.

3.3. Effects of Bacterial Concentration on Hydrogel Printability. After assessing the rheological properties of the bacterium-laden hydrogels, we evaluated the printability of the hydrogels under the same printing parameters. All bacterium-laden constructs were printed at a constant print speed of 5 mm s^{-1} and an extrusion rate of 0.6 mm^3 s^{-1} at 25 °C. The printing parameters were selected because higher extrusion rates resulted in structures with low pore factor (Pr) values, while lower extrusion rates resulted in discontinuous prints. As observed with the shear rheology measurements, increasing the bacterial concentration had minimal effects on the printability of the hydrogel constructs (Figure 4). To assess printability, we measured all printed constructs' line widths and pore factors. The pore factor is a dimensionless parameter used to define the print integrity of a printed structure. Pore factor values should approximate a value of 1 for structures with high print stability. When pore factor values are much less than 1 (Pr $\ll$ 1), this indicates that hydrogels are under-gelated, which then results in print structures that are too liquid-like (significant spreading). However, pore factor values much greater than 1 (Pr $\gg$ 1) indicate that hydrogels are over-gelated, thus resulting in discontinuous prints (broken filaments).[46−48] The following equation often defines the pore factor (eq 3)

https://doi.org/10.1021/acsbiomaterials.5c00223
ACS Biomater. Sci. Eng. 2025, 11, 3455−3466

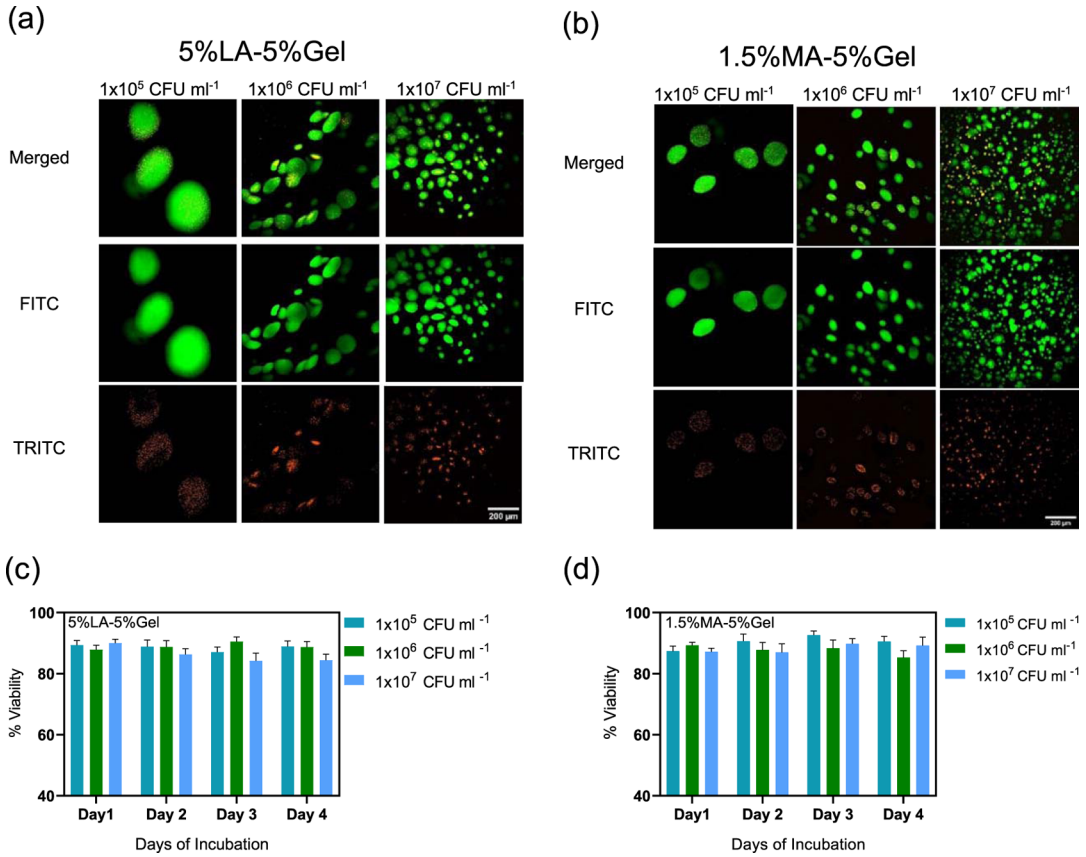

Figure 5. Viability of hydrogel-printed constructs over time. (a,b) Live/dead fluorescence microscopy assessment of day 4 *S.* Typhimurium microcolonies in 5%LA−5%Gel and 1.5%MA−5%Gel hydrogels obtained using 20× magnification (scale bar = 200 μm). (c,d) Quantitative assessment plots of microcolonies showing bacteria maintaining viability >80% for all days of incubation.

$$\mathrm{Pr} = \frac{L^2}{16A} \tag{3}$$

where L and A represent the perimeter and area, respectively. Here, hydrogels constructed with a bacterial concentration greater than 1×10^7 CFU mL^{-1} were not evaluated due to low shear viscosity and unstable print characteristics. Pore factors for increasing bacterial concentration were measured to be 1.02, 0.96, 0.97, and 0.96 for the 5%LA−5%Gel hydrogels encapsulated with 0, 1×10^5, 1×10^6, and 1×10^7 CFU mL^{-1}, respectively (Table S3). Similarly, 1.5%MA−5%Gel hydrogels exhibited a pore factor of 0.96, 0.92, 0.92, and 0.88 for the same bacterial seeding concentrations. All hydrogels exhibit stable print characteristics with pore factor Pr ∼ 1; however, we note a slight decrease in pore factor values with increasing bacterial concentrations.

3.4. Effects of Bacterial Concentration on Viability and Biofilm Formation. We assessed the viability of the encapsulated bacteria in both the 5%LA−5%Gel and 1.5% MA−5%Gel hydrogels for a four-day incubation period (Figure 5). Fluorescent live/dead images were taken for four different regions of the printed structures, and our results showed that the developed bacterial microcolonies were widely distributed in the hydrogel (Figures 5 and 6). Results show that the growth of *S.* Typhimurium follows a similar trend in both hydrogel environments, where viability is maintained above 80% for the four-day incubation period (Figure 5c,d). When comparing the viability of the bacteria in the 5%LA−5% Gel and the 1.5%MA−5%Gel hydrogels, we observed no significant difference in the overall viability in both gels throughout the 4 day incubation time (Figure 5c,d). We also observed that hydrogels with lower bacterial initial seeding density (1×10^5 CFU mL^{-1}) form larger microcolonies with an average area ranging from 13,093 μm^2 on day 1 of incubation to 30,339 μm^2 by day 4 which is about 4 orders of magnitude larger than the average area of microcolonies of hydrogels initially seeded with the higher bacterial concentrations (1×10^7 CFU mL^{-1}) (Figure 6c) in the 5%LA−5% Gel hydrogels.

Overall, we observe that the average microcolony area is larger for bacteria encapsulated in the 5%LA−5%Gel hydrogel, which has a cross-linked modulus of 4.7 kPa, compared to the 1.5%MA−5%Gel hydrogel with a cross-linked modulus of approximately 2.7 kPa. However, a similar trend is observed for both hydrogels, where the average microcolony area increases with a decreasing initial bacterial concentration. The average microcolony size in the 1.5%MA−5%Gel hydrogels for the low initial bacterial seeding concentration ranges from 9609.69 μm^2 on day 1 to 17310.4 μm^2 by day 4 of incubation (Figure 6c). Moreover, to characterize the morphology of the bacterial aggregates in the hydrogel, we quantitatively assessed the aggregate's circularity across the different incubation days (Figure 6f,g). While the size of the aggregates depends on both matrix properties and initial bacterial seeding density, circularity measurements depict that changes in aggregate shape are more dependent on the initial bacterial seeding concentration in the hydrogel environments, where we observed higher circularity values for the higher initial cell concentrations (1×10^7 CFU mL^{-1}) for the first 3 days of

https://doi.org/10.1021/acsbiomaterials.5c00223
ACS Biomater. Sci. Eng. 2025, 11, 3455−3466

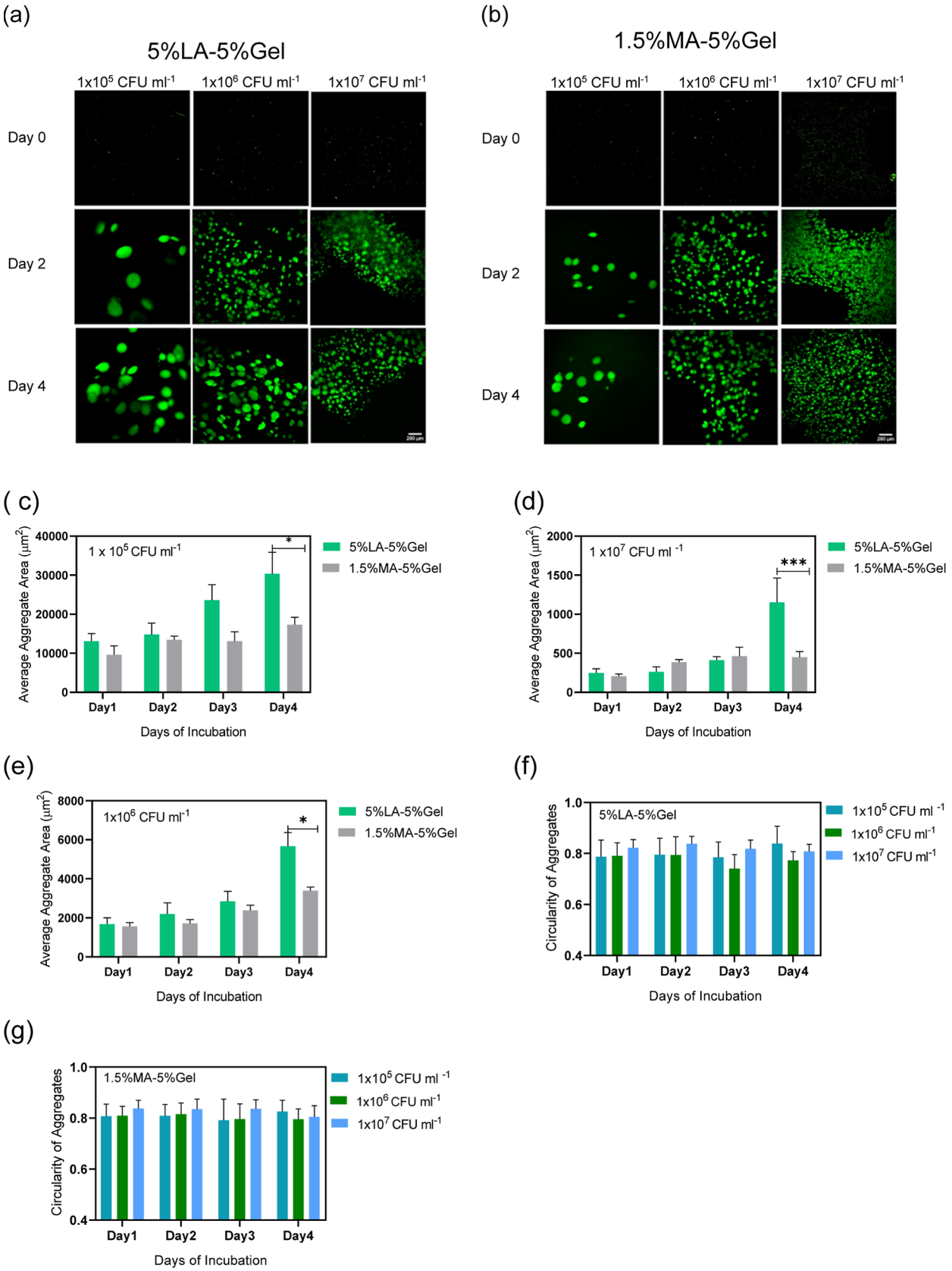

Figure 6. Morphology changes and developments of bacterial aggregates in 5%LA−5%Gel and 1.5%MA−5%Gel hydrogel-printed constructs over time. (a,b) Fluorescence microscopy assessment of *S.* Typhimurium microcolonies in 5%LA5%Gel and 1.5%MA5%Gel hydrogels obtained using 10× magnification from day 0 to day 4 of the culture period (scale bar = 200 μm). (c−e) Quantitative assessments of average microcolonies show that the bacterial aggregate size increases over time. However, the average size is higher for each initial bacterial seeding density in the 5%LA5%Gel hydrogels. (f,g) Circular plots of aggregates in both hydrogels indicate that the aggregates' morphology depends on the initial cell seeding concentration of bacteria. *$p < 0.05$ and ***$p < 0.001$.

https://doi.org/10.1021/acsbiomaterials.5c00223
ACS Biomater. Sci. Eng. 2025, 11, 3455−3466

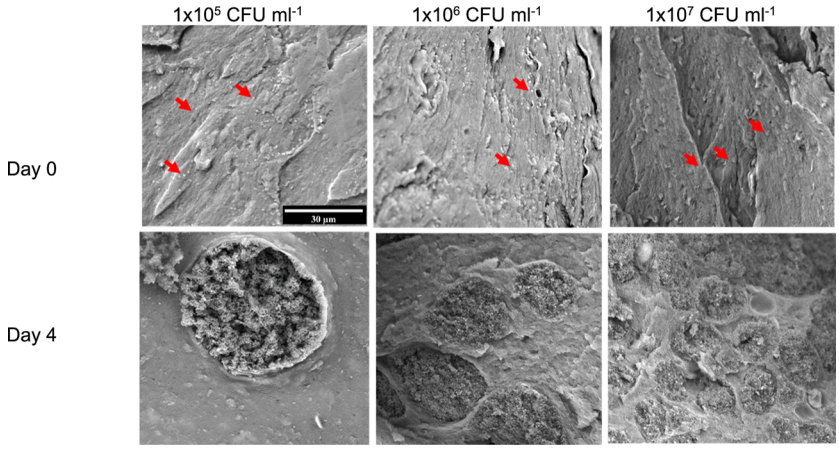

Figure 7. SEM images of varying concentrations of *S.* Typhimurium encapsulated in 5%LA−5%Gel hydrogels before incubation (day 0) and after 4 days of incubation (day 4). Images display *S.* Typhimurium as individual cells in a hydrogel environment on day 0. After 4 days of incubation, cells developed into large, densely packed microcolonies within the hydrogel with varying sizes and distribution based on the initial bacterial seeding concentration (scale bar = 30 μm). Red arrows point to cells in the hydrogel matrix.

incubation in both hydrogel environments. Finally, in Figure 7, we show that on day 0 before incubation, *S.* Typhimurium cells are individual cells dispersed in the hydrogel environment. However, after 4 days of incubation, these cells developed as large, densely packed bacterial communities deeply integrated within the hydrogel matrix environment. We also note that due to distinctive differences in the size of microcolony formation in both hydrogels, since the microcolony size is more extensive in the 5%LA−5%Gel hydrogel, it undergoes faster degradation than the 1.5%MA−5%Gel hydrogels where the printed structure of the 5%LA−5%Gel gels disintegrates during the 4 day culture period, whereas the 1.5%MA−5%Gel gels are better maintained.

4. DISCUSSION

In vitro, biofilm models formed in 3D create more representative models than traditional 2D cultures. These 3D models canmimic the behavior of naturally occurring biofilms that form within soft tissue-like environments, providing valuable insights for biomedical applications. In this work, we highlighted the effects of varying concentrations of *S.* Typhimurium on hydrogel viscoelastic properties for 3D printing applications. Before exploring the impact of bacterial encapsulation, we ensured that both hydrogel types exhibited similar viscoelastic properties in their precursor states. Rheological analysis confirmed that the formulated hydrogels have overlapping elastic moduli and shear-thinning behavior. This initial step was crucial for establishing a baseline for further investigations and accurately assessing the impact of varying bacterial concentrations on the hydrogel properties. Post-crosslinking with $CaCl_2$, we observed differences in the elastic and loss moduli between the two hydrogel types. The 5%LA−5%Gel hydrogels were twice as stiff as the 1.5%MA−5%Gel hydrogels. The difference in hydrogel stiffness can be attributed to the differences in the polymer chain lengths and polymer content of the 5%LA−5%Gel hydrogel and 1.5%MA−5%Gel hydrogels. Additionally, we show that while exhibiting a higher stiffness after crosslinking, the 5%LA−5%Gel has a faster stress relaxation time than the 1.5%MA−5%Gel, which may be attributed to the alginate polymer molecular weight difference. Existing literature has shown that the polymer molecular weight affects the polymer system's stress relaxation behavior, whereas lower-molecular-weight polymers exhibit faster stress relaxation behaviors.[45,49,50] Thus, our results demonstrate the effect of alginate molecular weight on gelation kinetics and the mechanical properties of hydrogels.[51,52]

While previous reports have explored the role of different factors, such as nutrients, on the viscoelastic properties of bacteria-encapsulated hydrogels,[38] there is limited understanding of the effects of varying bacteria's initial seeding densities. Evaluating the effects of bacterial cell loading on rheology, we examined four concentrations of *S. typhimurium* encapsulated in the alginate-gelatin hydrogels of various molecular weights. Up to an initial seeding concentration of 1×10^7 CFU mL^{-1}, the hydrogel viscoelasticity remained relatively unaltered, indicating that bacteria did not significantly affect the initial mechanical characteristics of the hydrogels. However, the storage modulus decreased considerably at the highest bacterial concentration (1×10^{10} CFU mL^{-1}), and shear-thinning behaviors became more pronounced. This response suggests that high bacterial concentrations modulate the microstructure of the gel, potentially influencing the overall hydrogel mechanical integrity and performance (Figure 3b,d), regardless of the hydrogel composition. Our findings align with previous studies that investigated the impact of bacterial concentrations on hydrogel rheology. Work by by Zhao et al. evaluated the effects of photosynthetic bacterial concentrations on hydrogel properties for wound healing applications, revealing similar trends of decreased storage and loss modulus with increasing bacterial concentrations.[53] Similarly, Kandemir et al. demonstrated that incorporating a concentration of bacteria equivalent to 1% of the total agarose hydrogel volume results in decreased hydrogel elastic modulus; however, different effects were observed for different species and the culture conditions evaluated.[38] These findings also align with the trends of increasing mammalian cells in hydrogel systems for tissue engineering applications,[35,36,54] where increasing cell concentrations decrease hydrogel viscosity.

Bioinks undergo shear deformation during extrusion, affecting their print resolution and ability to maintain a desired pore structure.[47] Here, we observed that the printability of the hydrogels remained largely unaffected by the initial seeding bacterial concentrations up to 1×10^7 CFU

https://doi.org/10.1021/acsbiomaterials.5c00223
ACS Biomater. Sci. Eng. 2025, 11, 3455−3466

mL^{-1}. The structural integrity and fidelity of the printed hydrogel constructs were maintained at this high initial cell concentration. This result is encouraging for bioprinting applications that aim to incorporate live bacteria into constructs for specific functionalities, such as bioactive wound dressings or engineered tissues with tailored microbiomes. After printing, we assessed the viability and morphological changes of the biofilms within the hydrogels. Cellular aggregates within 5%LA−5%Gel and 1.5%MA−5%Gel hydrogels exhibited high viability, with levels above 80% maintained throughout the 4 day incubation period. Interestingly, we observed that larger biofilm aggregates formed in hydrogels with lower initial bacterial seeding concentrations. Previous works aiming to assess external mechanics' effects on biofilm growth in confined environments have primarily focused on using a single, dilute concentration of bacteria and have demonstrated the development of larger ordered colonies in stiffer environments.[37,55] However, our results have shown that microcolonies' growth and size in confined environments also depend on the bacterial concentration in the confined space.

Moreover, the 5%LA−5%Gel hydrogels consistently exhibited larger biofilm aggregates across all initial bacterial seeding concentrations in comparison to the 1.5%MA−5%Gel hydrogels. The formation of large bacterial colonies within hydrogels has been linked to mechanisms, such as restricted motility, depletion aggregation, and bridging aggregation. Staudinger et al. showed that *P. aeruginosa* encapsulated in high-polymer-concentration agar and mucus hydrogels formed larger microcolonies due to restricted motility, limiting bacterial movement and forcing cells into localized clusters.[56] Similarly, Secor et al. identified depletion and bridging interactions as key drivers of bacterial aggregation in polymer matrices.[57] Depletion aggregation dominates at high polymer and cell concentrations, where entropy-driven forces pack cells together, while bridging aggregation occurs at high polymer concentrations but low cell densities, where polymer chains form connections between individual cells, effectively "bridging" them into clusters. While these mechanisms explain aggregation behavior, hydrogel stiffness and stress relaxation also play crucial roles. Zhang et al. demonstrated that matrix stiffness influences biofilm morphology and bacterial spatial arrangement.[37] Stress relaxation, which determines how the matrix responds to applied stress over time, has been shown to modulate cellular behavior. Faster stress relaxation has been shown to enhance cell proliferation in 3D mammalian culture by accommodating cellular forces.[45,49,50] Valentin et al. reported that *E. coli* adhered more to softer, viscous-like substrates with longer relaxation times.[58] However, Han et al. observed reduced microcolony size for *E. coli* and *Staphylococcus aureus* in stiffer methacrylate alginate hydrogels, highlighting the complexity of these interactions.[59] Here we have observed a similar interplay between the hydrogel stiffness and stress relaxation. The stiffer 5%LA−5%Gel hydrogel exhibited a faster stress relaxation than the softer 1.5MA−5%Gel hydrogel. This combination of high stiffness and rapid relaxation likely created a favorable environment for larger bacterial aggregates. The faster stress relaxation in the stiffer hydrogel may enable the polymer network to readily accommodate bacterial-induced forces, supporting both depletion and bridging aggregation mechanisms. Additionally, the unique stress relaxation behavior of the 5%LA−5%Gel may mimic aspects of soft-tissue-like environments, which could further enhance aggregation. Understanding how bacteria−matrix bidirectional interactions and matrix mechanical characteristics modulate bacterial survival, microcolony shape, and surrounding 3D environments is necessary for future *in vitro* applications.[60]

5. CONCLUSION

Here, we focused on the effects of bacterial concentrations on the alginate-based hydrogel rheology, printability, cell aggregation, and viability. Our findings reveal that low initial bacterial seeding concentrations, up to 1×10^7 CFU mL^{-1}, have minimal impact on the rheological properties of the hydrogel precursors. However, when the initial seeding concentration exceeded 1×10^7 CFU mL^{-1}, the hydrogel precursors exhibited more pronounced shear-thinning behavior and reduced printing resolution. This observation highlights the importance of carefully controlling the bacterial loading in hydrogel formulations to maintain optimal rheological characteristics for extrusion-based biofabrication. We also assessed the biofilm growth behavior in 3D confined environments. We highlighted that both the initial bacterial seeding concentrations and matrix rigidity influence biofilm growth, where we observed larger biofilm clusters with lower bacterial seeding concentrations in hydrogels with higher stiffness and stress relaxation behavior. These findings hold significant promise for advancing the design of biomaterials in diverse biomedical applications, such as tissue engineering, wound healing, and bioprinting, where controlling the interplay between hydrogels and bacteria is crucial for achieving the desired therapeutic outcomes. Insights gained from this work may pave the way for mechanically tuned hydrogel-based biofilm systems for advanced healthcare applications.

■ ASSOCIATED CONTENT

Supporting Information

The Supporting Information is available free of charge at https://pubs.acs.org/doi/10.1021/acsbiomaterials.5c00223.

Rheology of hydrogels crosslinked with 5% $CaCl_2$ without the encapsulation of *S. typhimurium* (Figure S1), stress-relaxation fitting parameters for crosslinked hydrogels without bacteria encapsulation (Table S1), fitting parameters for the power-law model for 5%LA−5%Gel and 1.5%MA−5%Gel hydrogel samples (Table S2), and printability assessment for hydrogel systems with increasing initial seeding densities (Table S3) (PDF)

■ AUTHOR INFORMATION

Corresponding Author

Jamel Ali − *Department of Chemical and Biomedical Engineering, FAMU-FSU College of Engineering, Tallahassee, Florida 32310, United States; National High Magnetic Field Laboratory, Tallahassee, Florida 32310, United States;* orcid.org/0000-0002-2997-1981; Email: jali@eng.famu.fsu.edu

Authors

Annie Scutte − *Department of Chemical and Biomedical Engineering, FAMU-FSU College of Engineering, Tallahassee, Florida 32310, United States; National High Magnetic Field Laboratory, Tallahassee, Florida 32310, United States*

Kiram Harrison − *Department of Chemical and Biomedical Engineering, FAMU-FSU College of Engineering, Tallahassee, Florida 32310, United States; National High Magnetic Field Laboratory, Tallahassee, Florida 32310, United States*

Tyler Gregory − *Department of Chemical and Biomedical Engineering, FAMU-FSU College of Engineering, Tallahassee, Florida 32310, United States; National High Magnetic Field Laboratory, Tallahassee, Florida 32310, United States*

David Quashie, Jr. − *Department of Chemical and Biomedical Engineering, FAMU-FSU College of Engineering, Tallahassee, Florida 32310, United States; National High Magnetic Field Laboratory, Tallahassee, Florida 32310, United States*

Subramanian Ramakrishnan − *Department of Chemical and Biomedical Engineering, FAMU-FSU College of Engineering, Tallahassee, Florida 32310, United States; National High Magnetic Field Laboratory, Tallahassee, Florida 32310, United States*

Complete contact information is available at: https://pubs.acs.org/10.1021/acsbiomaterials.5c00223

Notes

The authors declare no competing financial interest.

■ ACKNOWLEDGMENTS

This work was funded by the National Science Foundation (CMMI-2000330, EES-2000202, EES-2306449, and EES-2219558) and supported by the NSF FAMU CREST Center award (EES-1735968). All the work was performed at the National High Magnetic Field Laboratory, which is supported by the National Science Foundation Cooperative Agreement No. DMR-2128556 and the State of Florida. This material is also based upon work supported by the Air Force Office of Scientific Research under award numbers FA9550-24-1-0353, FA8650-20-2-5853, and W911NF-24-1-0281. The views and conclusions contained in this document are those of the authors and should not be interpreted as representing the official policies, either expressed or implied, of the Air Force Office of Scientific Research or the U.S. Government. The U.S. Government is authorized to reproduce and distribute reprints for Government purposes, notwithstanding any copyright notation herein.

■ REFERENCES

(1) Su, Y. J.; Yrastorza, J. T.; Matis, M.; Cusick, J.; Zhao, S.; Wang, G. S.; Xie, J. W. Biofilms: Formation, Research Models, Potential Targets, and Methods for Prevention and Treatment. *Adv. Sci.* **2022**, *9* (29), No. e2203291.

(2) Muhammad, M. H.; Idris, A. L.; Fan, X.; Guo, Y. C.; Yu, Y. Y.; Jin, X.; Qiu, J. Z.; Guan, X.; Huang, T. P. Beyond Risk: Bacterial Biofilms and Their Regulating Approaches. *Front. Microbiol.* **2020**, *11*, 928.

(3) Harrell, J. E.; Hahn, M. M.; D'Souza, S. J.; Vasicek, E. M.; Sandala, J. L.; Gunn, J. S.; McLachlan, J. B. Salmonella Biofilm Formation, Chronic Infection, and Immunity Within the Intestine and Hepatobiliary Tract. *Front. Cell. Infect. Microbiol.* **2021**, *10*, 624622.

(4) Rode, D. K. H.; Singh, P. K.; Drescher, K. Multicellular and unicellular responses of microbial biofilms to stress. *Biol. Chem.* **2020**, *401* (12), 1365−1374.

(5) Rumbaugh, K. P.; Sauer, K. Biofilm dispersion. *Nat. Rev. Microbiol.* **2020**, *18* (10), 571−586.

(6) Li, Z.; Wang, X. Y.; Wang, J.; Yuan, X. Y.; Jiang, X. Y.; Wang, Y. Y.; Zhong, C.; Xu, D. K.; Gu, T. Y.; Wang, F. H. Bacterial biofilms as platforms engineered for diverse applications. *Biotechnol. Adv.* **2022**, *57*, 107932.

(7) Mittrücker, H.-W.; Kaufmann, S. H. E. Immune response to infection with Salmonella typhimurium in mice. *J. Leukocyte Biol.* **2000**, *67* (4), 457−463.

(8) Zha, L.; Garrett, S.; Sun, J. Salmonella infection in chronic inflammation and gastrointestinal cancer. *Diseases* **2019**, *7* (1), 28.

(9) Vestby, L. K.; Grønseth, T.; Simm, R.; Nesse, L. L. Bacterial biofilm and its role in the pathogenesis of disease. *Antibiotics* **2020**, *9* (2), 59.

(10) Adcox, H. E.; Vasicek, E. M.; Dwivedi, V.; Hoang, K. V.; Turner, J.; Gunn, J. S. Salmonella extracellular matrix components influence biofilm formation and gallbladder colonization. *Infect. Immun.* **2016**, *84* (11), 3243−3251.

(11) Asp, M. E.; Ho Thanh, M. T.; Germann, D. A.; Carroll, R. J.; Franceski, A.; Welch, R. D.; Gopinath, A.; Patteson, A. E. Spreading rates of bacterial colonies depend on substrate stiffness and permeability. *PNAS Nexus* **2022**, *1* (1), pgac025.

(12) Lencova, S.; Svarcova, V.; Stiborova, H.; Demnerova, K.; Jencova, V.; Hozdova, K.; Zdenkova, K. Bacterial Biofilms on Polyamide Nanofibers: Factors Influencing Biofilm Formation and Evaluation. *ACS Appl. Mater. Interfaces* **2021**, *13* (2), 2277−2288.

(13) Warrier, A.; Satyamoorthy, K.; Murali, T. S. Quorum-sensing regulation of virulence factors in bacterial biofilm. *Future Microbiol.* **2021**, *16* (13), 1003−1021.

(14) Chen, D.; Cao, Y.; Yu, L.; Tao, Y.; Zhou, Y.; Zhi, Q.; Lin, H. Characteristics and influencing factors of amyloid fibers in S. mutans biofilm. *AMB Express* **2019**, *9*, 31.

(15) Fei, C. Y.; Mao, S.; Yan, J.; Alert, R.; Stone, H. A.; Bassler, B. L.; Wingreen, N. S.; Kosmrlj, A. Nonuniform growth and surface friction determine bacterial biofilm morphology on soft substrates. *Proc. Natl. Acad. Sci. U.S.A.* **2020**, *117* (14), 7622−7632.

(16) Cont, A.; Rossy, T.; Al-Mayyah, Z.; Persat, A. Biofilms deform soft surfaces and disrupt epithelia. *Elife* **2020**, *9*, No. e56533.

(17) Gomez, S.; Bureau, L.; John, K.; Chene, E. N.; Debarre, D.; Lecuyer, S. Substrate stiffness impacts early biofilm formation by modulating Pseudomonas aeruginosa twitching motility. *Elife* **2023**, *12*, No. e81112.

(18) Wang, L.; Wong, Y.-C.; Correira, J. M.; Wancura, M.; Geiger, C. J.; Webster, S. S.; Touhami, A.; Butler, B. J.; O'Toole, G. A.; Langford, R. M.; et al. The accumulation and growth of Pseudomonas aeruginosa on surfaces is modulated by surface mechanics via cyclic-di-GMP signaling. *npj Biofilms Microbiomes* **2023**, *9* (1), 78.

(19) Ferreira, F. A.; Souza, R. R.; Bonelli, R. R.; Américo, M. A.; Fracalanzza, S. E. L.; Figueiredo, A. M. S. Comparison of in vitro and in vivo systems to study ica-independent Staphylococcus aureus biofilms. *J. Microbiol. Methods* **2012**, *88* (3), 393−398.

(20) Balasubramanian, S.; Yu, K.; Cardenas, D. V.; Aubin-Tam, M.-E.; Meyer, A. S. J. Emergent biological endurance depends on extracellular matrix composition of three-dimensionally printed Escherichia coli biofilms. *ACS Synth. Biol.* **2021**, *10* (11), 2997−3008.

(21) James, G. A.; Swogger, E.; Wolcott, R.; Pulcini, E. D.; Secor, P.; Sestrich, J.; Costerton, J. W.; Stewart, P. S. Biofilms in chronic wounds. *Wound Repair Regen.* **2008**, *16* (1), 37−44.

(22) Bjarnsholt, T.; Jensen, P. Ø.; Fiandaca, M. J.; Pedersen, J.; Hansen, C. R.; Andersen, C. B.; Pressler, T.; Givskov, M.; Høiby, N. J. Pseudomonas aeruginosa biofilms in the respiratory tract of cystic fibrosis patients. *Pediatr. Pulmonol.* **2009**, *44* (6), 547−558.

(23) Pabst, B.; Pitts, B.; Lauchnor, E.; Stewart, P. S. Gel-entrapped Staphylococcus aureus bacteria as models of biofilm infection exhibit growth in dense aggregates, oxygen limitation, antibiotic tolerance, and heterogeneous gene expression. *Antimicrob. Agents Chemother.* **2016**, *60* (10), 6294−6301.

(24) Werthen, M.; Henriksson, L.; Jensen, P. Ø.; Sternberg, C.; Givskov, M.; Bjarnsholt, T. An in vitro model of bacterial infections in wounds and other soft tissues. *Apmis* **2010**, *118* (2), 156−164.

(25) Coquet, L.; Junter, G.; Jouenne, T. J. Resistance of artificial biofilms of Pseudomonas aeruginosa to imipenem and tobramycin. *J. Antimicrob. Chemother.* **1998**, *42* (6), 755−760.

(26) Kyle, S. 3D Printing of Bacteria: The Next Frontier in Biofabrication. *Trends Biotechnol.* **2018**, *36* (4), 340−341.

(27) Jain, P.; Kathuria, H.; Dubey, N. J. B. Advances in 3D bioprinting of tissues/organs for regenerative medicine and in-vitro models. *Biomaterials* **2022**, *287*, 121639.
(28) Harley, W. S.; Li, C. C.; Toombs, J.; O'Connell, C. D.; Taylor, H. K.; Heath, D. E.; Collins, D. J. Advances in biofabrication techniques towards functional bioprinted heterogeneous engineered tissues: A comprehensive review. *Bioprinting* **2021**, *23*, No. e00147.
(29) Labowska, M. B.; Cierluk, K.; Jankowska, A. M.; Kulbacka, J.; Detyna, J.; Michalak, I. A Review on the Adaption of Alginate-Gelatin Hydrogels for 3D Cultures and Bioprinting. *Materials* **2021**, *14* (4), 858.
(30) Liu, X. Y.; Inda, M. E.; Lai, Y.; Lu, T. K.; Zhao, X. H. Engineered Living Hydrogels. *Adv. Mater.* **2022**, *34* (26), 2201326.
(31) Muller, J.; Jakel, A. C.; Richter, J.; Eder, M.; Falgenhauer, E.; Simmel, F. C. Bacterial Growth, Communication, and Guided Chemotaxis in 3D-Bioprinted Hydrogel Environments. *ACS Appl. Mater. Interfaces* **2022**, *14* (14), 15871−15880.
(32) Ning, E.; Turnbull, G.; Clarke, J.; Picard, F.; Riches, P.; Vendrell, M.; Graham, D.; Wark, A. W.; Faulds, K.; Shu, W. M. 3D bioprinting of mature bacterial biofilms for antimicrobial resistance drug testing. *Biofabrication* **2019**, *11* (4), 045018.
(33) Aliyazdi, S.; Frisch, S.; Hidalgo, A.; Frank, N.; Krug, D.; Müller, R.; Schäfer, U. F.; Vogt, T.; Loretz, B.; Lehr, C.-M. 3D bioprinting of E. coli MG1655 biofilms on human lung epithelial cells for building complex in vitro infection models. *Biofabrication* **2023**, *15* (3), 035019.
(34) Liu, X.; Yuk, H.; Lin, S.; Parada, G. A.; Tang, T.-C.; Tham, E.; de la Fuente-Nunez, C.; Lu, T. K.; Zhao, X. 3D Printing of Living Responsive Materials and Devices. *Adv. Mater.* **2018**, *30* (4), 1704821.
(35) Diamantides, N.; Dugopolski, C.; Blahut, E.; Kennedy, S.; Bonassar, L. J. High density cell seeding affects the rheology and printability of collagen bioinks. *Biofabrication* **2019**, *11* (4), 045016.
(36) Schwartz, R.; Malpica, M.; Thompson, G. L.; Miri, A. K. Cell encapsulation in gelatin bioink impairs 3D bioprinting resolution. *J. Mech. Behav. Biomed. Mater.* **2020**, *103*, 103524.
(37) Zhang, Q. T.; Li, J.; Nijjer, J.; Lu, H. R.; Kothari, M.; Alert, R.; Cohen, T.; Yan, J. Morphogenesis and cell ordering in confined bacterial biofilms. *Proc. Natl. Acad. Sci. U.S.A.* **2021**, *118* (31), No. e2107107118.
(38) Kandemir, N.; Vollmer, W.; Jakubovics, N. S.; Chen, J. J. Mechanical interactions between bacteria and hydrogels. *Sci. Rep.* **2018**, *8* (1), 10893.
(39) Jana, S.; Charlton, S. G.; Eland, L. E.; Burgess, J. G.; Wipat, A.; Curtis, T. P.; Chen, J. J. Nonlinear rheological characteristics of single species bacterial biofilms. *npj Biofilms Microbiomes* **2020**, *6* (1), 19.
(40) Gregory, T.; Benhal, P.; Scutte, A.; Quashie, D.; Harrison, K.; Cargill, C.; Grandison, S.; Savitsky, M. J.; Ramakrishnan, S.; Ali, J. Rheological characterization of cell-laden alginate-gelatin hydrogels for 3D biofabrication. *J. Mech. Behav. Biomed. Mater.* **2022**, *136*, 105474.
(41) Muri, H. I.; Hoang, L.; Hjelme, D. R. J. A. S. Mapping nanoparticles in hydrogels: a comparison of preparation methods for electron microscopy. *Appl. Sci.* **2018**, *8* (12), 2446.
(42) Song, K.; Ji, L.; Zhang, J.; Wang, H.; Jiao, Z.; Mayasari, L.; Fu, X.; Liu, T. J. Fabrication and cell responsive behavior of macroporous PLLA/gelatin composite scaffold with hierarchical micro-nano pore structure. *Nanomaterials* **2015**, *5* (2), 415−424.
(43) Moran, P.; Coats, B. J. M. T. Biological sample preparation for SEM imaging of porcine retina. *Microsc. Today* **2012**, *20* (2), 28−31.
(44) Tan, J.; Luo, Y.; Guo, Y.; Zhou, Y.; Liao, X.; Li, D.; Lai, X.; Liu, Y. J. Development of alginate-based hydrogels: Crosslinking strategies and biomedical applications. *Int. J. Biol. Macromol.* **2023**, *239*, 124275.
(45) Chaudhuri, O.; Gu, L.; Klumpers, D.; Darnell, M.; Bencherif, S. A.; Weaver, J. C.; Huebsch, N.; Lee, H.-P.; Lippens, E.; Duda, G. N.; et al. Hydrogels with tunable stress relaxation regulate stem cell fate and activity. *Nat. Mater.* **2016**, *15* (3), 326−334.
(46) Kyle, S.; Jessop, Z. M.; Al-Sabah, A.; Whitaker, I. S. Printability'of candidate biomaterials for extrusion based 3D printing: state-of-the-art. *Adv. Healthcare Mater.* **2017**, *6* (16), 1700264.
(47) Ribeiro, A.; Blokzijl, M. M.; Levato, R.; Visser, C. W.; Castilho, M.; Hennink, W. E.; Vermonden, T.; Malda, J. J. B. Assessing bioink shape fidelity to aid material development in 3D bioprinting. *Biofabrication* **2018**, *10* (1), 014102.
(48) Ouyang, L.; Yao, R.; Zhao, Y.; Sun, W. J. B. Effect of bioink properties on printability and cell viability for 3D bioplotting of embryonic stem cells. *Biofabrication* **2016**, *8* (3), 035020.
(49) Hazur, J.; Endrizzi, N.; Schubert, D. W.; Boccaccini, A. R.; Fabry, B. Stress relaxation amplitude of hydrogels determines migration, proliferation, and morphology of cells in 3-D culture. *Biomater. Sci.* **2021**, *10* (1), 270−280.
(50) Bauer, A.; Gu, L.; Kwee, B.; Li, W. A.; Dellacherie, M.; Celiz, A. D.; Mooney, D. J. Hydrogel substrate stress-relaxation regulates the spreading and proliferation of mouse myoblasts. *Acta Biomater.* **2017**, *62*, 82−90.
(51) Szekalska, M.; Pucilowska, A.; Szymanska, E.; Ciosek, P.; Winnicka, K. Alginate: Current Use and Future Perspectives in Pharmaceutical and Biomedical Applications. *Int. J. Polym. Sci.* **2016**, *2016*, 1.
(52) Lee, K. Y.; Mooney, D. J. Alginate: properties and biomedical applications. *Prog. Polym. Sci.* **2012**, *37* (1), 106−126.
(53) Zhao, E.; Liu, H.; Jia, Y.; Xiao, T.; Li, J.; Zhou, G.; Wang, J.; Zhou, X.; Liang, X.-J.; Zhang, J.; et al. Engineering a photosynthetic bacteria-incorporated hydrogel for infected wound healing. *Acta Biomater.* **2022**, *140*, 302−313.
(54) Zhang, J. H.; Wehrle, E.; Adamek, P.; Paul, G. R.; Qin, X. H.; Rubert, M.; Muller, R. Optimization of mechanical stiffness and cell density of 3D bioprinted cell-laden scaffolds improves extracellular matrix mineralization and cellular organization for bone tissue engineering. *Acta Biomater.* **2020**, *114*, 307−322.
(55) Li, J.; Kothari, M.; Chockalingam, S.; Henzel, T.; Zhang, Q.; Li, X.; Yan, J.; Cohen, T. Nonlinear inclusion theory with application to the growth and morphogenesis of a confined body. *J. Mech. Phys. Solids* **2022**, *159*, 104709.
(56) Staudinger, B. J.; Muller, J. F.; Halldorsson, S.di.; Boles, B.; Angermeyer, A.; Nguyen, D.; Rosen, H.; Baldursson, O.; Gottfredsson, M.; Gudmundsson, G.dm. H.; Singh, P. K. Conditions Associated with the Cystic Fibrosis Defect Promote Chronic Pseudomonas Aeruginosa Infection. *Am. J. Respir. Crit. Care Med.* **2014**, *189* (7), 812−824.
(57) Secor, P. R.; Michaels, L. A.; Ratjen, A.; Jennings, L. K.; Singh, P. K. Entropically driven aggregation of bacteria by host polymers promotes antibiotic tolerance in Pseudomonas aeruginosa. *Proc. Natl. Acad. Sci. U.S.A.* **2018**, *115* (42), 10780−10785.
(58) Valentin, J. D. P.; Qin, X. H.; Fessele, C.; Straub, H.; van der Mei, H. C.; Buhmann, M. T.; Maniura-Weber, K.; Ren, Q. Substrate viscosity plays an important role in bacterial adhesion under fluid flow. *J. Colloid Interface Sci.* **2019**, *552*, 247−257.
(59) Han, Y.; Jiang, N.; Xu, H.; Yuan, Z.; Xiu, J.; Mao, S.; Liu, X.; Huang, J. Extracellular Matrix Rigidities Regulate the Tricarboxylic Acid Cycle and Antibiotic Resistance of Three-Dimensionally Confined Bacterial Microcolonies. *Adv. Sci.* **2023**, *10* (9), 2206153.
(60) Koo, H.; Yamada, K. M. Dynamic cell−matrix interactions modulate microbial biofilm and tissue 3D microenvironments. *Curr. Opin. Cell Biol.* **2016**, *42*, 102−112.

https://doi.org/10.1021/acsbiomaterials.5c00223
ACS Biomater. Sci. Eng. 2025, 11, 3455−3466